Effect of Geometric Granularity on the Noise Signature of a Full-Scale Large Civil Transport Nose Landing Gear

Ehab Fares[1] and Benedikt König[2]
Dassault Systèmes Deutschland GmbH, Stuttgart, D-70563, Germany

Mehdi R. Khorrami[3]
NASA Langley Research Center, Hampton, VA, 23681, USA

Results from a comprehensive simulation campaign focused on characterizing the airframe noise signature of a full-scale Boeing 777-300ER nose landing gear are presented. The as-flown, installed nose gear geometry was used to assess how accurately the selected computational methodology can predict far-field noise before extending the simulation approach to the complete B777-300ER aircraft in landing configuration. To facilitate direct comparisons with experimental data, the simulations were conducted for conditions matching those recorded for a flyby of the same aircraft over the ground-based phased microphone array used during the 2005 Quiet Technology Demonstrator II test. The far-field acoustic footprint of the nose landing gear was computed via a Ffowcs-Williams and Hawkings integral approach, with pressures on the model solid surface or flow quantities on a permeable data surface enclosing the gear used as input. A grid refinement study performed for the baseline gear configuration to establish the convergence behavior of the far-field spectrum indicated that the sound pressure levels had converged at frequencies slightly beyond 5 kHz for the finest spatial resolution attempted. To ascertain the effects of geometric granularity on far-field noise, simulations of a defeatured version of the nose gear were undertaken. Comparisons with fully-dressed gear results indicated that finer geometric details add 2–4 dB to the sound pressure levels at mid- to high-frequencies (800 Hz to 5 kHz), suggesting that for accurate noise prediction such details cannot be neglected.

I. Introduction

Landing gears and wing high-lift devices, such as slats and flaps, are the major airframe components that produce a significant portion of the noise affecting communities near the flight path of landing aircraft [1]. For large commercial transports, contributions from the landing gear to the total airframe noise signature increase substantially [2-4]. System-level, accurate, full-scale prediction of landing gear noise for large airliners is a very difficult task because of the extreme geometric complexity of the relevant components. Nonetheless, high-fidelity, simulation-based prediction of landing gear noise is essential to a deeper understanding of noise generation mechanisms and to the development of efficient noise abatement strategies. The work summarized here is part of a larger effort, first of its kind, to predict accurately the airframe noise characteristics of a full-scale, large civil transport in a landing configuration.

Taking advantage of the knowledge gained under the NASA Environmentally Responsible Aviation (ERA) and Flight Demonstrations and Capabilities (FDC) projects, the NASA-Boeing joint effort on airframe noise prediction was designed to extend simulation-based methodologies to the landing gear and high-lift systems of full-scale, large commercial transports. Executed over a four-year period, the collaboration proceeded as a series of steps whereby the complexity and relevance of the studied configuration to the full-scale, complete aircraft were gradually increased. A Boeing 777 aircraft was selected as the testbed due to availability of model- and full-scale experimental data for validation purposes.

---

[1] Director, Aerospace and Defense (currently with Geely Auto Technical, Deutschland, GmbH), Senior Member AIAA.
[2] Senior Technical Manager, Aerospace and Defense.
[3] Senior Scientist, Computational AeroSciences Branch, Associate Fellow AIAA

The collaboration commenced with simulations of a 26%-scale, high-fidelity B777-200 main landing gear (MLG) model in isolation. This proof-of-concept effort determined that the computational methodology was able to capture the far-field noise footprint and other relevant trends of an isolated, subscale MLG. These simulations produced results [5, 6] that were in excellent agreement with wind-tunnel acoustic measurements [7]. The simulations also demonstrated clearly that only flow variables computed on a permeable data surface can be used as input to a Ffowcs-Williams and Hawkings (FWH) integral method [8] to produce the correct far-field noise spectrum. That is, the less computationally intensive approach that uses fluctuating pressures calculated on the model solid surface as input to the FWH method significantly overpredicted the sound pressure levels (SPL). Therefore, the computational cost for all subsequent configurations was increased substantially, since the high-resolution region in the immediate vicinity of the model had to be extended to the permeable data surface.

Simulations of a 26%-scale, semispan B777-200 – also referred to as Subsonic Transport Aeroacoustic Research or STAR – model with main gear, slats, and flaps deployed (landing configuration) were undertaken in the next phase. This configuration enabled us to examine the accuracy of the aeroacoustic data predicted for the installed main gear and to validate the computations against available experimental measurements of the STAR model [9-11]. Full accounts of the simulation campaign targeting the semispan STAR model and validation of the simulated results are given in Refs. [12] and [13].

The third step was devoted to simulations of the full-scale, installed nose landing gear (NLG) of a B777-300ER aircraft in combination with a cruise wing. This configuration permitted close examination of issues that are critical to landing gear noise prediction. First, we had determined previously [14] that the forward location of the nose gear, away from other airframe components, precluded interactions among the noise contribution produced by this component and those from the main gear and high-lift devices. As a result, the setup for the effectively isolated nose gear enabled simulations at a very fine resolution that would have been prohibitive if the main gear were also deployed. By performing NLG simulations at successively finer resolutions, we were able to ascertain the full effect of spatial resolution on predicted sound levels and frequency content of the far-field spectrum. Second, this configuration was also used to develop a meshing strategy better suited to simulate the extremely challenging case of the full aircraft in a landing configuration. Finally, the installed NLG with cruise wing configuration provided an ideal opportunity to assess the effects of geometric granularity on the far-field noise signature of a full-scale landing gear design that is flown on current large civil transports.

Simulations performed during the last phase of the NASA-Boeing joint effort, which targeted the most challenging configurations – full-scale, complete B777-300ER aircraft with nose and main landing gear deployed and wing high-lift devices either stowed or deflected – are featured in Ref. [15].

The present paper describes the computational campaign executed in support of the third phase of the collaboration. Here, we analyze the simulated results for both baseline and defeatured versions of the NLG. Validation of the predicted noise signatures produced by the baseline NLG with microphone array measurements from flight tests of the same aircraft [4] is provided in Ref. [16].

II. Aircraft Configuration and Flight Conditions

A brief account of the simulated geometry is provided in this section. Also discussed are the steps followed to produce a less detailed (defeatured) version of the NLG configuration. A short description of the flight conditions emulated in the simulations is presented last.

A. Aircraft Configuration

A digital model of a full-scale, full-span B777-300ER was painstakingly developed by personnel of the NASA Langley Research Center (LaRC) Geometry Laboratory (GeoLab). The fuselage and most of the wing, including high-lift devices, were generated from the 26%-scale 777-200 (STAR) model. Geometry definitions for two fuselage extension plugs, horizontal and vertical tails, and wing outboard segments delivered by Boeing were used to convert the aircraft to a B777-300ER version. Since the main focus of the NASA-Boeing collaboration was landing gear noise, most of the resources were spent developing a CFD-ready CAD definition of the undercarriage from geometry files provided by Boeing that included the NLG and MLG bays. During this crucial phase, extreme care was exercised to ensure that the digital models faithfully replicated the full-scale landing gear as currently flown on B777-300ER aircraft. The simulated geometry is depicted in Fig. 1. Note from Fig. 1a that the geometry does not include nacelles and that only the NLG is deployed; observe from Fig. 1b that the open gear bay (cavity) is fully represented. As mentioned previously, this configuration permitted the careful examination of various issues relevant to landing gear noise prediction.

a) Simulated geometry b) Close-up of simulated NLG and gear bay

Fig. 1 Geometry of the Boeing 777-300ER large civil transport.

All finer details of the full-scale NLG geometry were maintained in the simulations through extensive use of automatic surface meshing and wrapping techniques available in the geometry preprocessor PowerDELTA©. An example of the level of detail considered in the digital model and corresponding simulations is shown in Fig. 2. Care was taken to ensure that these small-scale features were properly resolved.

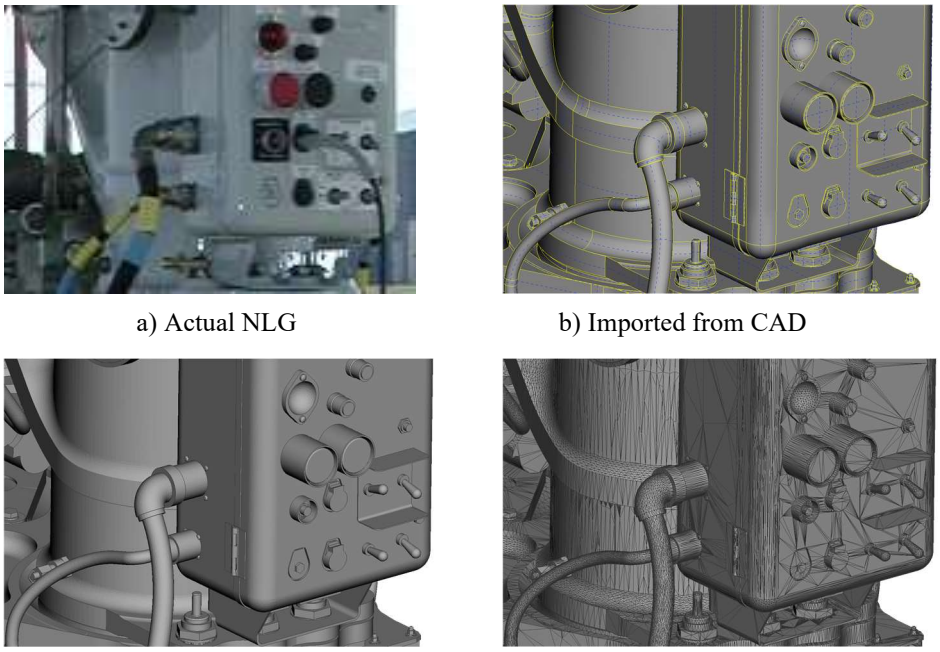

a) Actual NLG b) Imported from CAD

c) Used in simulation d) Surface mesh representation

Fig. 2 Geometry detail of full-scale NLG.

The full-scale NLG developed for the present simulations includes the finest level of geometric detail ever considered by the authors of this study or of any other found in the open literature. Unresolved questions for the airframe noise community are whether such geometric granularity is necessary, and if so, what are its effects on the intensity and frequency content of the far-field noise spectrum. To address these questions, a defeatured version of the NLG was generated. A relevant simplification of such a complex geometry requires a substantial manual effort spanning several steps. As a first step, the gear hydraulic lines, cables, and a host of other very fine structures that could be easily eliminated were removed. Simulation of the resulting simplified NLG geometry failed to produce meaningful changes in the levels or character of the far-field noise spectrum. In the following step, additional finer features were eliminated without significantly smoothing the subcomponents that included these features. Simulation of the ensuing geometry produced changes in the narrow-band spectral levels of 1–2 dB in the mid- to high-frequency (800 Hz to 5

kHz) range. Although measureable, these changes were deemed insufficient to draw any meaningful conclusions. A proper level of simplification was produced by removing or smoothing out additional geometric details and by resurfacing some of the larger components. Sample close-up views of the defeatured NLG are displayed in Figs. 3 through 7. The objective of this simplification process was to achieve a level of geometric granularity that represents a landing gear at an earlier design stage when such details are usually missing. A defeatured gear geometry can also be evaluated in terms of the gains in computational efficiency and overall solution turn-around time for the desired accuracy.

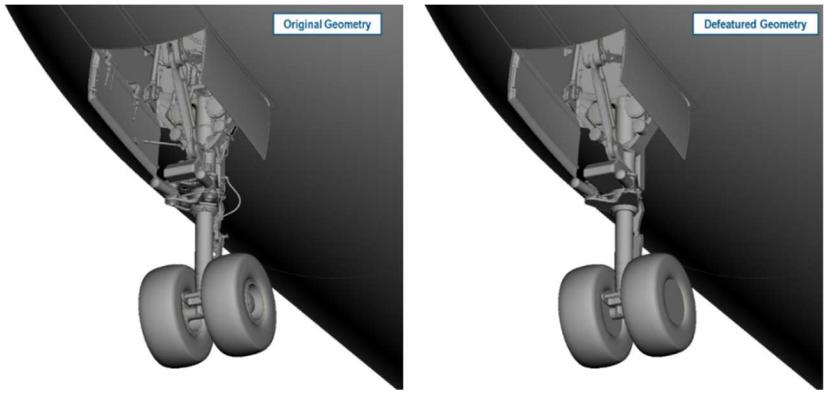

a) General view from below

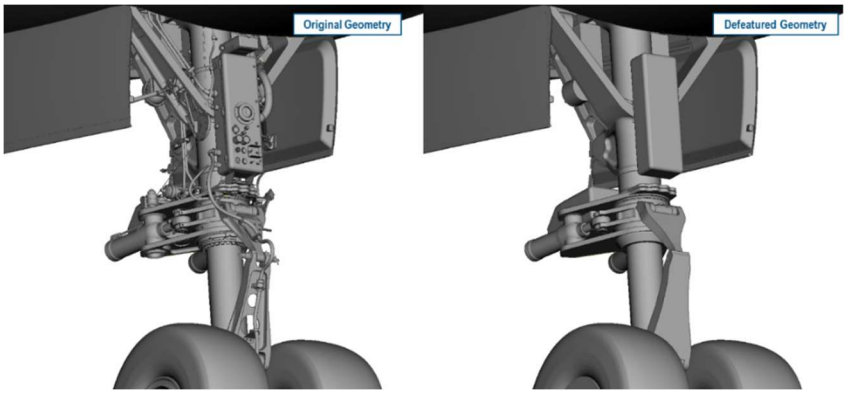

b) Close-up view from rear

Fig. 3 Simplification of B777-300ER NLG geometry – global view.

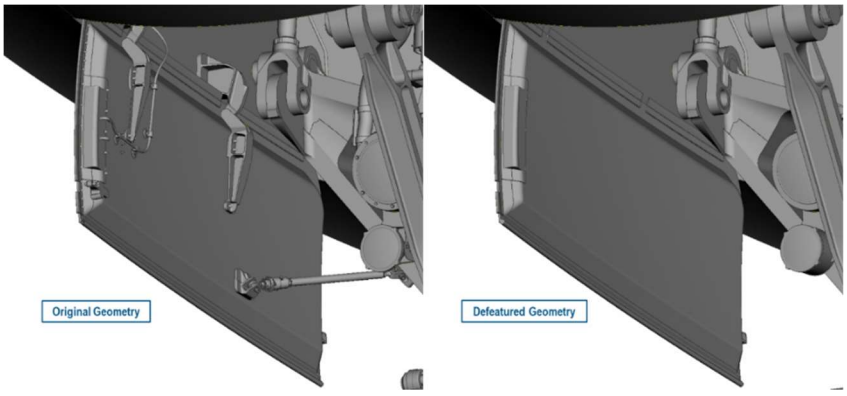

Fig. 4 Simplification of B777-300ER NLG geometry – wheel bay.

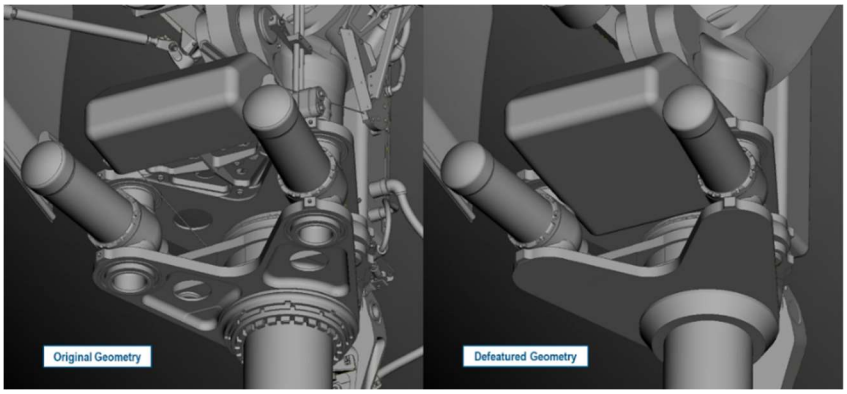

Fig. 5 Simplification of B777-300ER NLG geometry – steering mechanism.

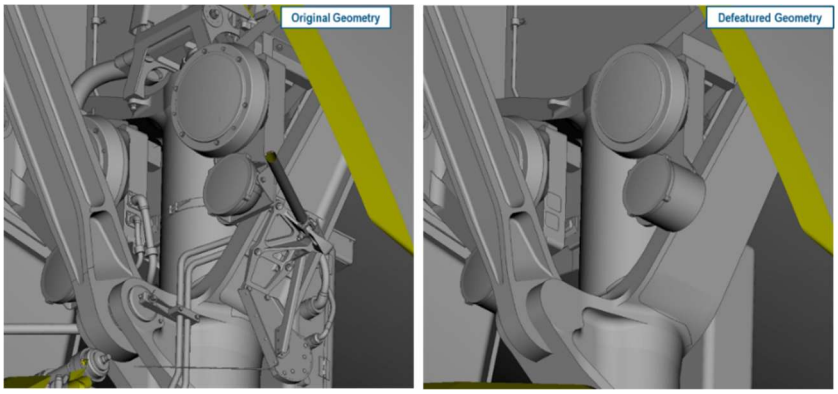

Fig. 6 Simplification of B777-300ER NLG geometry – lighting system.

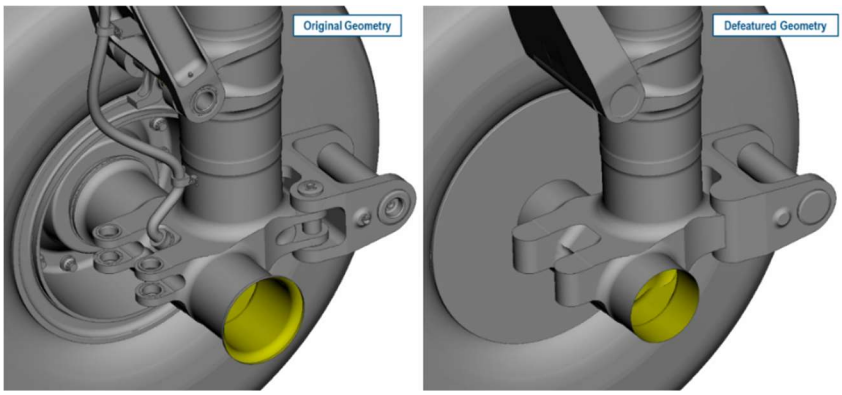

Fig. 7 Simplification of NLG B777-300ER geometry – wheel axle region.

B. Flight Conditions

With the exception of Reynolds number (Re), the simulations were performed at flight conditions and aircraft parameters that matched those recorded during a microphone array pass of the aircraft with cruise wing and the landing gear deployed, performed during the 2005 Quiet Technology Demonstrator II (QTD2) test [4]. The Re for all computations was 20×10^6, which is approximately 35% of the flight Re based on mean aerodynamic chord (MAC) and aircraft speed of 230 kts.[4] This Re is sufficiently high to produce far-field noise levels that are nearly equivalent, at a lower computational cost, to those obtained at full flight Re [17]. A schematic representation of the aircraft orientation

[4] Equivalently, Re = 20×10^6 is approximately 50% of the flight Re based on MAC and an aircraft landing speed of 160 kts.

relative to the microphone array on the ground is given in Fig. 8. Corresponding input conditions for the configuration with a deployed landing gear and a cruise wing are listed in Table 1. Pitch and flight path angles were used to determine the effective angle of attack and the correct geometric position of the microphone array relative to the aircraft.

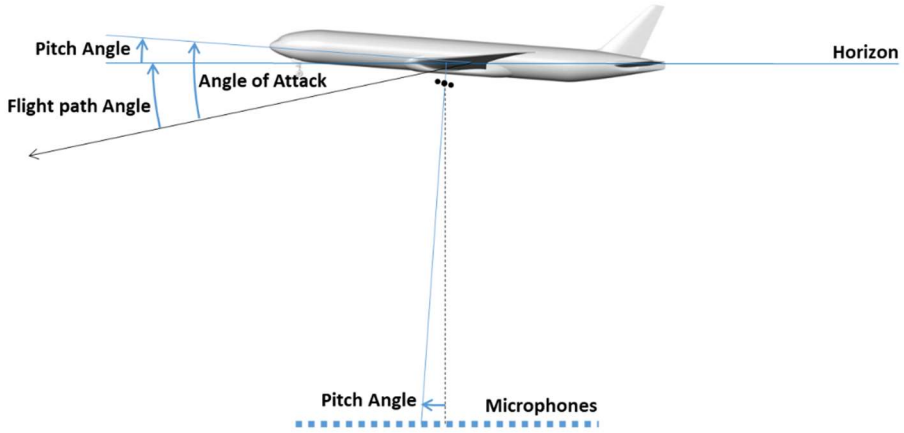

Fig. 8 Geometric relations (far-field distance not to scale).

Table 1. Flight conditions used for simulations of selected aircraft configuration.

Configuration	Angle of Attack, AOA	M	Speed (kts)	Re
gear deployed, cruise wing	6.5°	0.344	229.8	20×10^6

III. Computational Approach

The numerical simulations were performed with a commercial flow solver from Dassault Systemes, PowerFLOW®, which uses a three-dimensional, 19 state (D3Q19) formulation of the lattice Boltzmann method (LBM). Results from this solver have been validated for numerous aerodynamic [18-21] and aeroacoustic [5, 17, 22-24] applications related to airframe noise prediction for model- and full-scale aircraft in landing configurations. Advantages of the simulation technique include simplicity in discretizing real-world, detailed geometries; ease in generating meshes that can be tailored to desired spatial accuracy and frequency range requirements; low numerical dispersion and dissipation properties [25]; and efficient execution on massively parallel computers.

A. Turbulence Modeling

Resolution of all turbulence length scales in a direct numerical simulation (DNS), using either traditional Navier-Stokes or LBM flow solvers, is limited to low Re [26, 27]. Large eddy simulation (LES), and even the considerably cheaper wall-modeled large eddy simulation (WMLES) approaches, are still far away from simulating a full aircraft at or near flight Re. Hybrid methods for turbulent flow prediction, such as the family of detached eddy simulation (DES) [26] concepts, facilitated the extension of high-fidelity, unsteady simulations to more complex geometries. Turbulence modeling approaches based on DES are still regarded as the only feasible concepts to accurately capture turbulent phenomena involving separated flows [26-28]. The lattice Boltzmann very large eddy simulation (LB-VLES) [29, 30] methodology employed in PowerFLOW® [31-33] is also a hybrid approach where turbulence is modeled in wall-bounded, attached flows and mainly resolved in regions of separated flow. To reduce spatial resolution requirements for high Re flows near walls, a hybrid wall function is used to model the boundary layer on solid surfaces. The wall function model [34] is an extension of the standard log law of the wall, including the effects of laminar sublayers and pressure gradients, either favorable or adverse. An overview of the turbulence-resolving approach implemented in PowerFLOW® is provided in Ref. [29].

B. Grid Generation and Wall Treatment

The integration domain is discretized spatially in Cartesian volume elements (Voxels) that are refined locally in arbitrarily predefined variable resolution regions (VR). This arrangement allows local mesh refining and coarsening by factors of 2. The solid geometry represented through a facetized surface intersects the voxels and generates multiple surface elements (Surfels) that are utilized to define the appropriate slip and no-slip boundary conditions. This formulation [35] of the boundary condition on a curved surface cutting the Cartesian grid is automatically mass, momentum

and energy conservative while maintaining the general spatial second-order accuracy of the underlying LBM numerical scheme. Fully automatic generation of the volume mesh over realistic geometries, combined with high accuracy of the boundary condition implementation, are two important advantages of the LBM approach as implemented in PowerFLOW®.

C. Simulation Setup

The present simulations were performed for the full-scale aircraft in free-air at actual conditions for the Mach number and close to 35% of flight Re based on the aircraft speed listed in Table 1. Deployment of the NLG precluded usage of a symmetry plane, and thus, the full aircraft was simulated. Far-field boundary conditions were imposed at a distance of 20 fuselage lengths with several regions of far-field sponge zones defined with growing effective viscosity to dampen acoustic wave reflections. All simulations were initialized with free stream characteristic values, except for an offset region surrounding the NLG and filling the gear cavity. This region was initialized with zero velocity to provide a better initial condition and avoid large unsteadiness in the cavity at the start of each simulation.

The time-accurate simulations were conducted for a total of 2.5 seconds of physical time, corresponding to approximately 42 flow passes over the MAC or about 4 flow passes along the fuselage. The flow was allowed to settle for the first 1.5 seconds, where forces, moments and nearfield probes were considered statistically converged. The last second of physical time was used for data acquisition, to average the flow for calculation of aerodynamic forces and to sample the data for subsequent acoustic postprocessing at 27 kHz–90 kHz, depending on spatial resolution (extra coarse, coarse, medium, or fine). The data acquisition period was extended for one coarse simulation to confirm that 1 s is indeed sufficient to reach statistical convergence of the near-field flow and the far-field noise spectra.

Additional low- and high-frequency flow data were collected for animation and unsteady flow analysis purposes. Directly resolved high-frequency pressure probes were positioned in the flow domain at various distances away from the Ffowcs-Williams and Hawking (FWH) permeable data surface in the overhead and sideline directions relative to the NLG. Special care was exercised to ensure that proper spatial resolution was maintained to accurately capture wave propagation from the noise source to these probes. The locations of these probes in the overhead position, represented by red crosses, are displayed in Fig. 9a. Although they increased the computational costs (as will be shown later), these probes were critical in determining which FWH data surface was better suited for far-field noise calculations.

D. Far-field Noise Solver and Choice of FWH Integration Surface

Propagation of acoustic information to the far field was performed using a solution of the Ffowcs-Williams and Hawking (FWH) analogy developed by Farassat (formulation 1A, Ref. [8]), as implemented in PowerACOUSTICS® [36]. This time-domain implementation can accommodate flow convection and propagation for solid and permeable data surfaces. The use of Formulation 1A to propagate acoustic information from near-field, time-accurate flow solutions has been applied previously to similar airframe noise simulations [17] and validated successfully against wind tunnel [5] and flight test data [23]. Of interest to the airframe noise community [5, 37-39] is whether to use as input into FWH formulations the pressure field on aircraft solid surfaces or flow data on permeable surfaces to obtain accurate far-field noise results. Since generation of low-speed airframe noise is mainly a dipole-dominated mechanism, the common assumption that a solid surface formulation suffices is followed generally. However, inclusion of quadrupole-type volumetric effects such as diffraction and shielding, possible only with the permeable data surface FWH formulation, improves the accuracy of far-field noise spectra substantially, especially for realistically complex geometries [5, 40].

Far-field noise computations based on solid surface data typically achieve higher frequency content due to enhanced spatial resolution in the regions adjacent to the surface. Additionally, solid-surface-based FWH has been used to infer contributions to the far-field sound from individual surfaces. While the FWH computation based on permeable surfaces captures more physical effects, it has disadvantages when compared to solid-surface FWH. Among these is a usually lower frequency resolution that stems from the prohibitively high cost associated with a sufficiently increased spatial resolution within the volume enclosed by the permeable surface to properly capture wave propagation. Also, the choice of permeable data surface shape and position is not unique, and numerical experimentation is generally required to determine the best option. Ideally, this data surface should be closed and located outside the nonlinear flow region. Practically, a surface encompassing all noise sources with sufficient distance from them is chosen. The surface sometimes is left open to allow hydrodynamic fluctuations, such as wakes, to pass without generating artificial low-frequency noise in the FWH computation. An alternative approach is multiple cap averaging [41]. In this approach, the distributed pressure and velocity fields are recorded on several closely-spaced parallel planes in the wake region and averaged to minimize hydrodynamic effects typically observed at low frequencies. This technique has been used effectively for jet flows [41].

The FWH permeable data surface around the NLG and its end caps are indicated by the purple and black lines in Figs. 9a and 9b, respectively. This surface was carefully chosen to include all flow fluctuations produced by the NLG and highlighted in Fig. 9b as the isosurface of 1% standard deviation of velocity magnitude fluctuations. The surface has seven end caps used for flow averaging. The number of end caps had a minor effect on far-field noise propagation at overhead observer positions. Several permeable surface sizes were investigated to determine the most efficient without sacrificing accuracy. We observed during the exercise that intersecting the aircraft with the permeable surface did not affect the far-field spectrum at the observer positions analyzed.

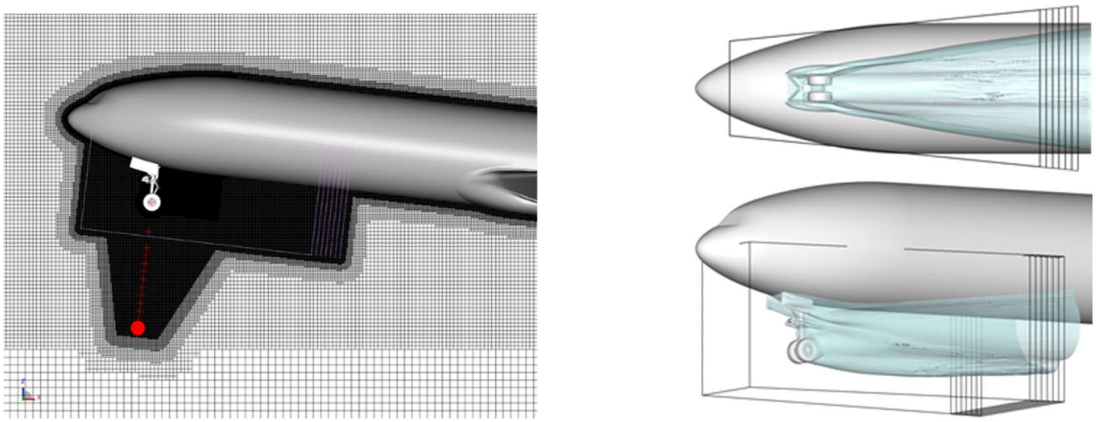

a) Mesh at center plane showing VRs b) Isosurface of standard deviation of velocity fluctuations

Fig. 9 Computational mesh and porous data surface for NLG.

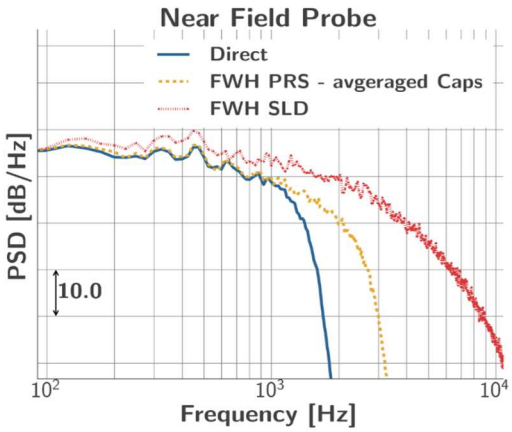

Fig. 10 Pressure spectra at near-field probe for an extra coarse simulation.

A comparison of power spectral density (PSD) spectra from permeable and solid surface FWH computations with the spectrum extracted directly from a computational probe (red solid circle in Fig. 9a) in the near field is shown in Fig. 10. Observe from the figure that the permeable, or porous, surface formulation (FWH PRS) produces a better match with the direct computational probe, except for differences at high frequencies caused by numerical diffusion effects imposed on the direct probe results as the waves travel the distance from the permeable surface to the probe. A comparison in the sideline direction produced similar results (not shown). The trends noted in Fig. 10 reaffirm our previous conclusion [5] that only flow variables computed on a permeable data surface around a landing gear should be used as input to an FWH integral method [8] to produce the correct far-field noise spectrum. Therefore, only this surface will be used for further analysis.

Observe also from Fig. 10 that, as expected, the solid surface (FWH SLD) generates overall higher pressure levels at high frequencies due to higher spatial resolution. In addition, note that the levels are also higher at mid and low frequencies when compared to the direct probe. Simulations with a closed cavity indicated that this effect is not related to trapped cavity modes. The observed overproduction of pressure fluctuations in the solid surface results could be related to the assumption of flow uniformity in the near field when accounting for convection effects on far-field noise. Since some of the NLG components are exposed to local velocities much lower than the uniform value, this assumption does not apply everywhere, and it may introduce cumulative errors in the all-important phase information.

IV. Numerical Results

A. Global View of the Flow

The flow over the collection of bluff bodies that constitute the NLG is characterized by an expansive turbulent separation area comprised of vortical structures of varying size and strength, as depicted by the isosurfaces of total pressure and vorticity presented in Figs. 11a and 11b, respectively. Note from Fig. 11b the presence of two counter-rotating vortices, generated at the bottom edges of the wheel bay doors, which convect within the NLG wake. The

free shear layer that forms when the incoming boundary layer separates at the forward lip of the open cavity impinges on the upper structures of the gear and may interact with the trailing edge of the cavity, potentially causing the excitation of a typical Rossiter mode resonance.

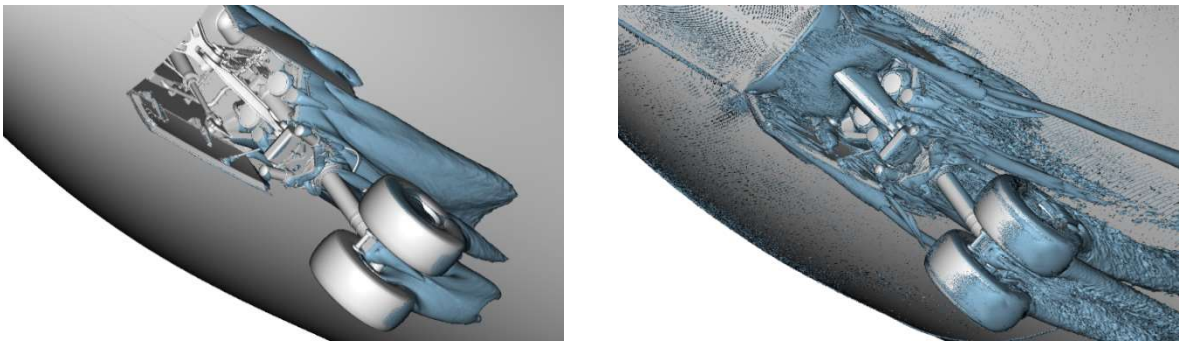

a) Total pressure (averaged flow field) b) Vorticity field (λ_2)

Fig. 11 Isosurfaces of flow past the NLG.

Sufficient spatial resolution was used to characterize the separated flow behind the landing gear (see Fig. 12), also corresponding to the volume enclosed by the porous data surface used in the FWH integral approach. The large-scale, turbulent flow structures were resolved and captured as shown in the planar images of Fig. 12, obtained from our medium-resolution simulation. In particular, note that the wheel axle area (Fig. 12b) produces a strong vortex-shedding mechanism that, as will be shown later, causes the tonal components in the predicted spectra. The sound waves generated as vortices shed from upstream components impinge on downstream elements within this region are qualitatively captured in Fig. 13a, where wave patterns that radiate forward at approximately 430 Hz are shown. The figure also depicts other wave patterns that reside inside the gear cavity. Figure 13b displays surface pressure contours (in dB) at a higher frequency of about 3700 Hz. The contours indicate, qualitatively, that high-amplitude pressure fluctuations exist in the axle region between the wheels. Note that higher-amplitude surface pressure fluctuations do not necessarily translate into far-field noise, but they may indicate areas responsible for noise generation.

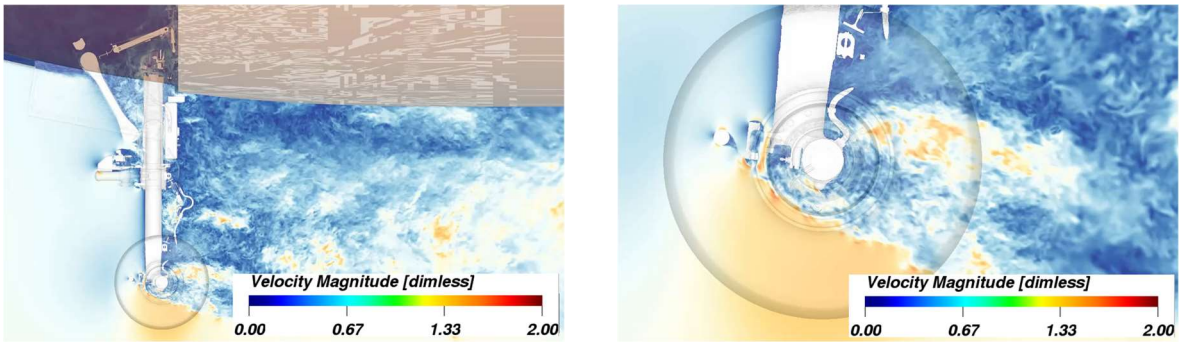

a) Wake of NLG b) Wheel axle area

Fig. 12 Instantaneous velocity magnitude. Simulation at medium spatial resolution.

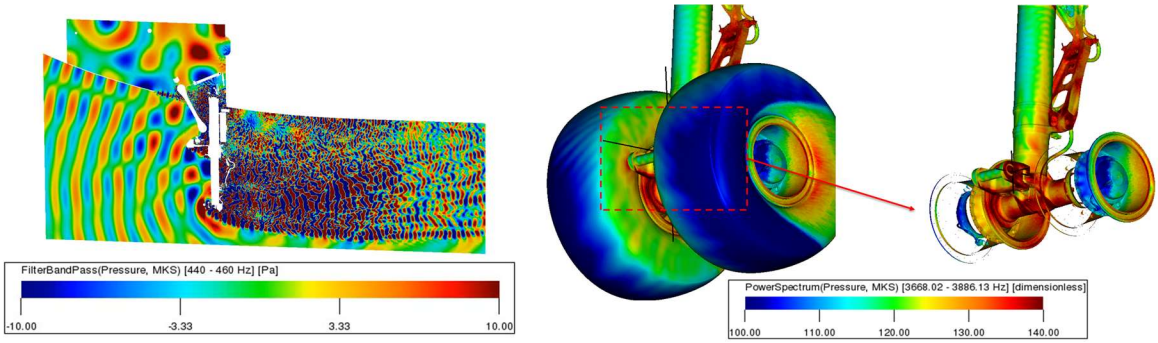

a) Band-filtered pressure field (450 Hz) b) Surface pressure (dB) at 3700 Hz.

Fig. 13 Instantaneous pressure contours in NLG wheel region.

B. Grid Resolution Study

An assessment of spatial resolution effects on solution behavior is an important element of any computational study. When considering numerous fine-scale geometric structures, as is the case here, such an assessment is essential. Four grid resolutions with a refinement factor of 1.5 in minimum global voxel size were used to simulate the flow around the baseline NLG. Simulation parameters for the four grids are summarized in Table 2. Corresponding simulations for the defeatured NLG geometry were performed up to the medium resolution. All simulations were conducted for the same initial flow conditions and physical time period. Since the computational effort rises with resolution with an exponent between three and four (cubic for the three spatial dimensions and an additional factor from the decrease in time step), there is a significant increase in the computational resources needed at higher spatial resolutions. For example, note from Table 2 that the number of voxels increased from less than one billion to 20 billion and the number of surfels from 60 million to 365 million when the extra coarse grid was refined to obtain the fine resolution grid. As mentioned earlier, the large voxel count arises from the necessity to use a porous FWH data surface to compute the far-field noise spectrum over a broad frequency range.

Table 2 Statistics for grid resolution study.

LCT Fullspan NLG	Resolution						
	Extra coarse		Coarse		Medium		fine
Minimum cell size [mm]	1.4		0.94		0.62		0.42
timesteps (for 2.5s) [10^6]	1.06		1.59		2.38		3.57
Geometry	Original	Defeatured	Original	Defeatured	Original	Defeatured	Original
Voxels [10^9]	0.86	0.83	2.1	2.0	6.4	6.2	20
FeV [10^9]	0.17	0.15	0.4	0.36	1.2	1.1	3.6
Surfels [10^6]	60	51	104	90	191	167	365
FeS [10^6]	20	13	34	23	62	32	118
CPUh [1k]	~80	~78	~350	~330	~1500	~1300	~4500

Due to the structure of time advancement implemented within PowerFLOW, voxels and surfels at the finest grid level (first level) are computed at each time step, second level elements are updated every second timestep, the third level elements every fourth timestep, etc. A representative case size that takes into account the different number of updates per timestep is given by fine equivalent voxels (FeV) and fine equivalent surfels (FeS), which provide an averaged number of volume and surface element updates per timestep.

Far-field PSD plots for several directivity angles in the flyover direction are depicted in Fig. 14. The spectra, calculated at the ground approximately 500 ft. from the aircraft, are given for both narrow and 1/3rd octave bands.

Results shown for all resolutions confirm that good convergence of the low- and mid-frequency segments of the spectra was achieved, with convergence extending to higher frequencies as the resolution increased. Based on spectral collapse at mid to high frequencies, up to about 5 kHz seem well resolved with the finest grid.

Scrutiny of the collected data indicated that the NLG wheel axle region produces the peaks in the spectra at 450 Hz and 900 Hz, whereas the cavity is the most likely cause of the tonal hump at 220 Hz in the forward (50°) and overhead (90°) directivities. The narrow peak at approximately 3.7 kHz was also traced to the wheel axle region (see Fig. 13b), and becomes visible only at medium and fine grid resolutions when higher frequencies were resolved properly. Note also from Fig. 14 that the magnitude of the peaks in the spectral plots is sensitive to resolution and behaves in a nonlinear fashion. Similar trends were observed in previous studies [42], where a small variation in the velocity field could cause certain flow mechanisms to enhance or reduce resonance patterns.

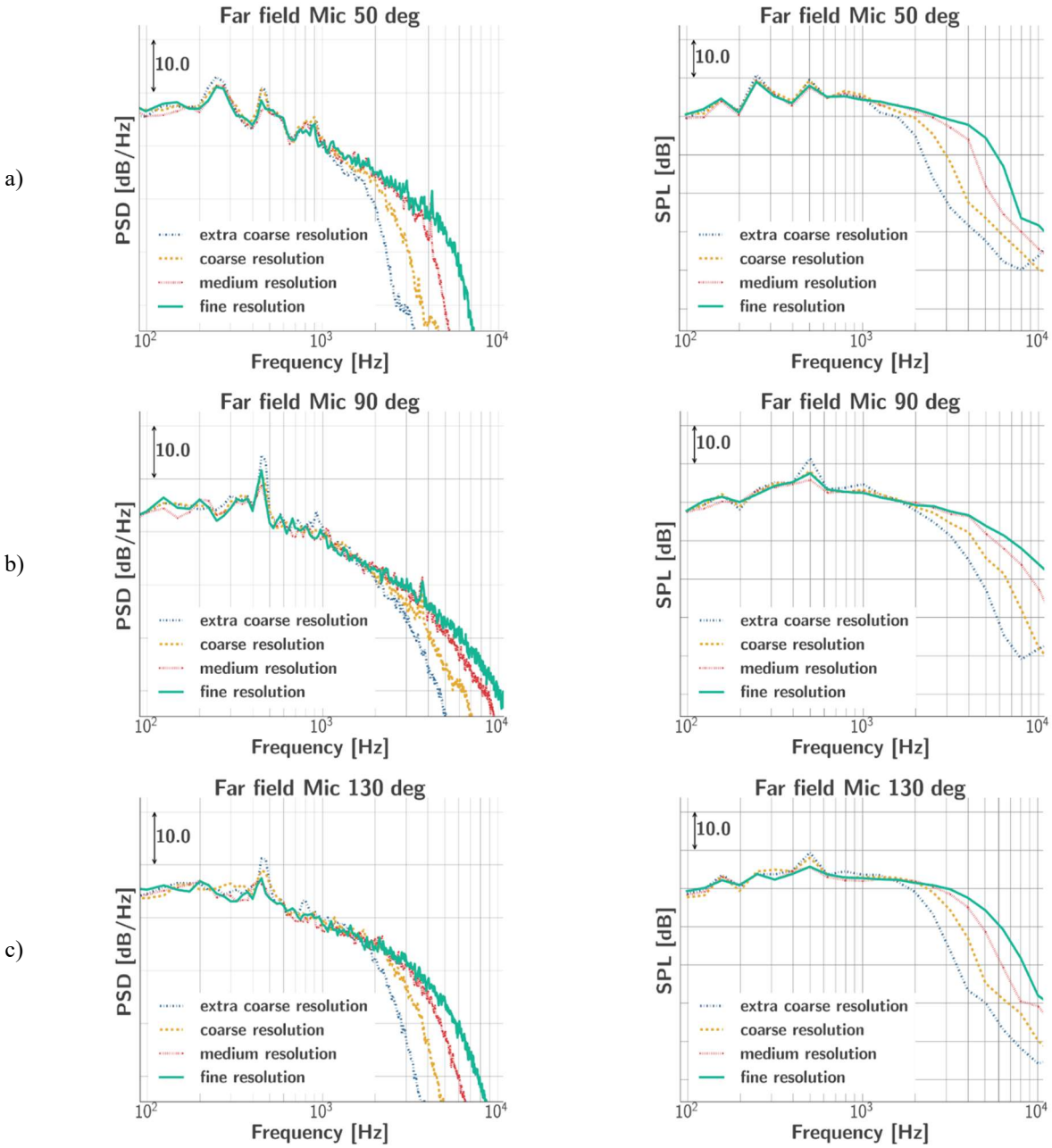

Fig. 14 Far-field spectra in the flyover direction at various directivity angles.

D-weighted (dBD) overall sound pressure levels (OASPL) are depicted in Fig. 15. This metric, which attenuates the effect of low-frequency noise and increases the effect of high-frequency noise in a manner approximating the behavior of the human ear, is used during aircraft noise certification. To compute OASPL, the spectra were integrated over the frequency range of 50 Hz to 2.5 kHz, which is the primary range of interest for published QTD2 flight test data [4]. Note from Fig. 15 that OASPL obtained from medium and fine resolution simulations fall within approximately 1 dBD of each other over a broad range of directivity angles in the flyover direction, indicating convergence of the far-field noise spectrum. Therefore, simulations on the medium resolution grid are adequate for predicting far-field noise within the selected frequency range.

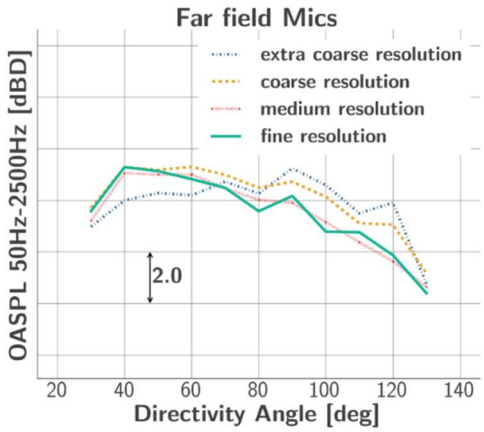

Fig. 15 Overall sound pressure level directivity of the far-field microphone linear array

C. Effect of Geometric Granularity

The simulation statistics summarized in Table 2 indicate that the NLG with lower geometric granularity (defeatured) reduces overall mesh size, especially the number of elements on the surface, and hence the computational effort. However, note that the overall reduction is minor because spatial resolution is driven by the target frequency range and is only weakly dependent on the actual geometry used. After the labor-intensive defeaturing task, automation of volume meshing, adaptation setup, and simulation processes within PowerFLOW® facilitated execution of the cases needed to assess the effects of geometric granularity up to medium spatial resolution. As shown in Fig.16, the qualitative differences in flow features between the baseline and defeatured NLG geometries are minor. One can argue, however, that the differences in geometric granularity alter blockage effects and produce an NLG wake that is moderately different in terms of its extent and regions of high velocity variation.

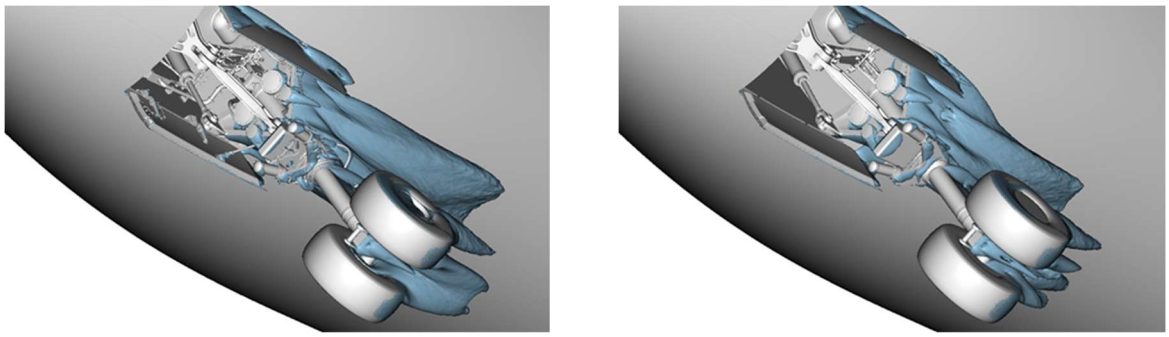

a) Isosurface of total pressure

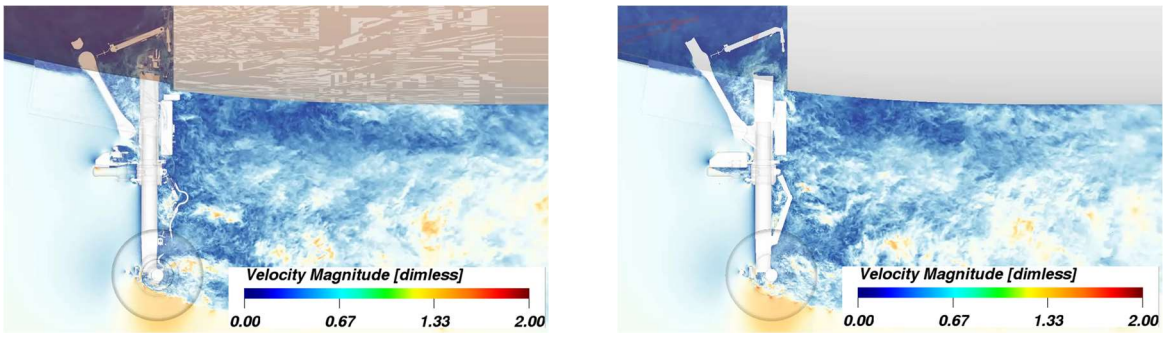

Baseline Defeatured

b) Instantaneous velocity magnitude at symmetry plane

Fig. 16 Flow in the wake of the NLG (medium spatial resolution).

In general, the defeatured geometry solution converged with spatial resolution similar to the baseline gear. A comparison of far-field spectra in narrow and 1/3rd-octave bands at two directivity angles is presented in Fig. 17. The figure clearly demonstrates that the defeatured NLG produces a far-field noise signature that possesses the main features and overall shape of the spectra associated with the baseline gear. Nevertheless, differences emerge in the low-, mid-, and high-frequency ranges: at low frequencies, the defeatured geometry produces sound pressure levels that are consistently higher than those for the baseline geometry. This may be a result of geometry streamlining, which could cause the wakes produced by the upstream subcomponents to convect and impinge on the downstream elements at higher velocities. The trend is reversed for high frequencies, where the baseline geometry produces higher sound pressure levels with some tonal features. This behavior seems to confirm the prevailing view that the smaller geometric features produce the smaller flow structures that cause high frequency noise. The comparison at medium frequencies indicates a subtle shift in frequency and change of magnitude of the peaks, confirming the previously identified sensitivity of these noise generation mechanisms to spatial resolution and local flow features.

a)

b)

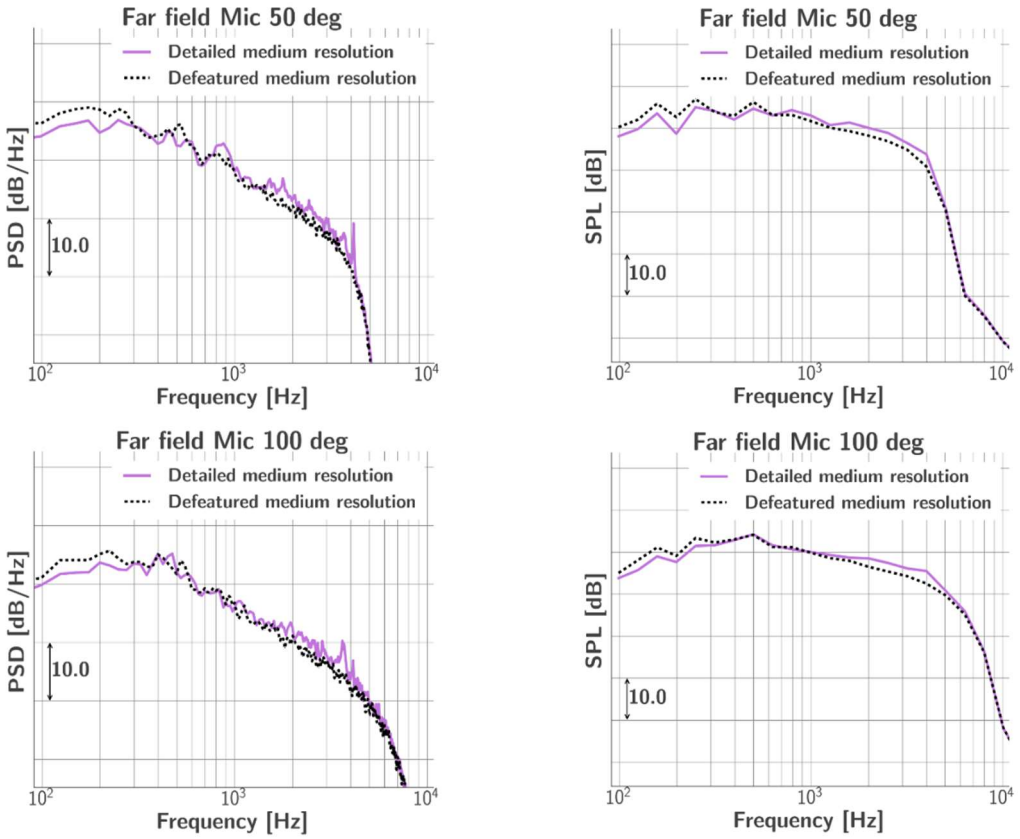

Narrow band PSD

Sound pressure level (1/3 octave band)

Fig. 17 Far-field spectra in the flyover direction at two directivity angles.

The OASPL for the frequency range 50 Hz–2.5 kHz is plotted in Fig. 18 for the baseline and defeatured NLG. Note that, depending on the metric used to make the comparison, lower frequencies for the dB metric or high frequencies for the dBD metric, dominate the OASPL. The differences are generally within 1dB/0.5dBD, which indicate good repeatability. However, the integrated wide band of the OASPL masks the true effects of geometric granularity observed in Fig. 17.

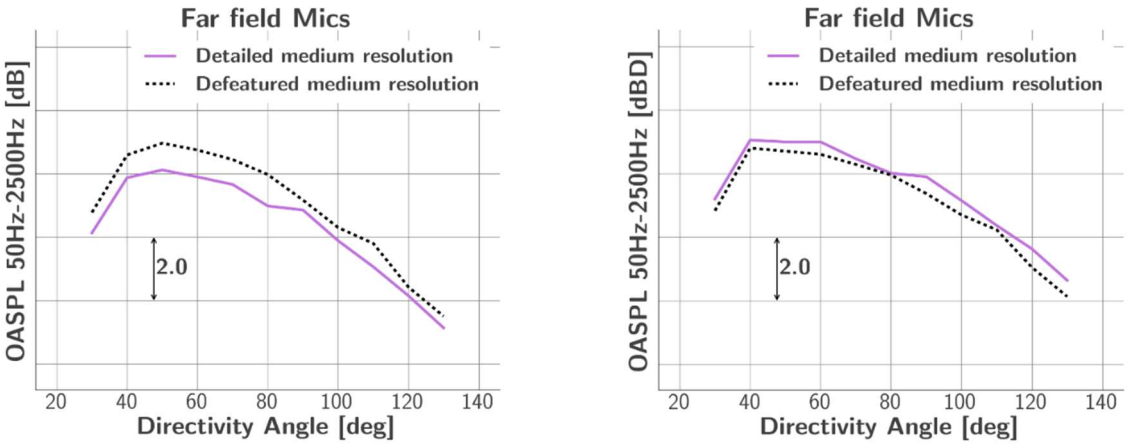

a) SPL, dB b) SPL, dBD

Fig. 18 Overall sound pressure level directivity at the far-field microphone linear array.

V. Summary and Outlook

High fidelity airframe noise simulations for two full-scale, realistic nose landing gear geometries with different geometric granularity and installed on a full aircraft were performed at different spatial resolutions. The flow features were documented and noise sources responsible for peaks and humps in the far-field spectra were identified. The spatial resolution study showed good grid convergence behavior with increasing high frequency content for increasing resolution. Based on the observed spectral collapse at high frequencies, the finest spatial resolution used in the simulations was sufficient to resolve radiated sound up to 5 kHz in full-scale. Medium resolution OASPL was within approximately1dBD of the values obtained at fine resolution in the frequency range 50 Hz – 2.5 kHz.

The granularity of the geometry had a small effect on wake flow and produced an increase/decrease in far-field noise spectra with opposite trends for low- and high-frequency ranges. The OASPL was within 1dB/0.5dBD for both baseline and defeatured NLG geometries. Except for the labor required to reduce the granularity of the geometry, the documented simulation process was easily repeatable, and the lower granularity geometry reduced the computational effort only by a small amount.

In conclusion, lower geometric granularity representative of landing gear designs at earlier stages of development can be used to understand flow behavior and highlight potential noise sources, especially tonal components, as long as relevant geometric details are present and resolved. A priori decisions on geometry removal or simplification require expertise and the process of defeaturing an existing, as-flown landing gear is labor-intensive. Elimination of an important noise-generating mechanism through geometric simplification is a risk in this manual process. Therefore, high-fidelity geometry and a high level of spatial resolution continue to be recommended for a reliable assessment of far-field noise, especially if small geometric variations are present in low-noise designs.

Acknowledgments

This work was supported by the FDC project under the Integrated Aviation Systems Program of the NASA Aeronautics Research Mission Directorate. We would like to express our sincere appreciation to Michael Czech and other personnel from the Boeing Company for their assistance in gathering and providing the CAD files of the as-flown B777-300ER nose and main landing gears. The authors also gratefully acknowledge the invaluable contribution of Scott Brynildsen of Craig Technologies for his patience with the tedious task of cleaning and integrating the various aircraft components into a CFD-ready digital representation, as well as providing geometry modifications and CAD support. In addition, the authors would like to thank Jason Appelbaum and Benjamin Duda of Dassault Systemes (formerly Exa Corporation) for their support during preparation of the initial surface mesh and computational setup. All simulations were performed on the Pleiades supercomputer at the NASA Advanced Supercomputing (NAS) facility at the Ames Research Center. The logistical support provided by NAS staff, in particular Yan-tyng (Sherry) Chang, is greatly appreciated.

References

[1] Dobrzynski, W., "Almost 40 Years of Airframe Noise Research: What Did We Achieve," J. Aircraft, Vol. 47, No. 2, March-April 2010, pp. 353–367.

[2] Chow, L. C., Mau, K., and Remy, H., "Landing Gears and High Lift devices Airframe Noise Research," AIAA Paper 2002-2408, June 2002.

[3] Stoker, R., Guo, Y., Streett, C., and Burnside, N., "Airframe Noise Source Locations of a 777 Aircraft in Flight and Comparisons with Past Model Tests," AIAA Paper 2003-3232, May 2003.

[4] Elkoby, R., Brusniak, L., Stoker, R., Khorrami, M. R., Abeysinghe, A., and Moe, J.W., "Airframe Noise Results from the QTD II Flight Test Program," AIAA Paper 2007-3457, May 2007.

[5] Koenig, B., Fares, E. Ravetta, P. A., and Khorrami, M. R., "A Comparative Study of Simulated and Measured Main Landing Gear Noise for Large Civil Transports," AIAA Paper 2017-3013, June 2017.

[6] Ravetta, P. A., Khorrami, M. R., Koenig, B., and Fares, E., "Analysis of Simulated and Experimental Noise Sources of the Boeing 777 Main Gear Model via CLEAN in 3D," AIAA Paper 2018-3417, June 2018.

[7] Ravetta, P. A., Khorrami, M. R., Burdisso, R. A., and Wisda, D. M., "Acoustic Measurements of a Large Civil Transport Main Landing Gear Model," AIAA Paper 2016-2901, May-June 2016.

[8] Ffowcs Williams, D. L. and Hawking, J. E., "Sound Generation by Turbulence and Surfaces in Arbitrary Motion," Philosophical Transactions of the Royal Society of London, Series A, Mathematical and Physical Sciences, Vol. 264, No. 1151, 1969, pp. 321–342.

[9] Horne, W. C., Burnside, N. J., Soderman, P. T., Jaeger, S. M., Reinero, B. R., James, K. D., and Arledge, T. K., "Aeroacoustic Study of a 26%-scale Semispan Model of Boeing 777 in the NASA Ames 40- by 80-Foot Wind Tunnel," NASA Technical Paper 2004-212802, October 2004.

[10] Storms, B. L., James, K. D., Satran, D., R., Arledge, T. K., Burnside, N. J., Horne, C. W., and Driver, D. M., "Aerodynamics of a 26%-scale Semi-span Model of the Boeing 777 in the NASA Ames 40- by 80-Foot Wind Tunnel," NASA Technical Paper 2005-212829, January 2005.

[11] Horne, W. C., James, K. D., Arledge, T. K., Soderman, P. T., Burnside, N., and Jaeger, S. M., "Measurements of 26%-scale 777 Airframe Noise in the NASA Ames 40- by 80-Foot Wind Tunnel," AIAA Paper 2005-2810, May 2005.

[12] Koenig, B., Fares, E., and Khorrami, M. R., "Aeroacoustic Study of a Subscale Large Civil Transport (STAR) Model – Part 1: Simulations," paper to be presented at the 27th AIAA/CEAS Aeroacoustics Conference, August 2021.

[13] Khorrami, M. R., Koenig, B., and Fares, E., "Aeroacoustic Study of a Subscale Large Civil Transport (STAR) Model – Part 2: Validation of Simulated Results," paper to be presented at the 27th AIAA/CEAS Aeroacoustics Conference, August 2021.

[14] Duda, B., Ferris, R. J., and Khorrami, M. R., "Simulation-Based Assessment of a Full-Scale Installed Quiet Landing Gear," AIAA Paper 2019-2476, May 2019.

[15] Khorrami, M. R., Koenig, B., Fares, E., Ribeiro, A. F. P., Czech, M., and Ravetta, P., "Airframe Noise Simulations of a Full-Scale Large Civil Transport in Landing Configuration," paper to be presented at the 27th AIAA/CEAS Aeroacoustics Conference, August 2021.

[16] Czech, M., Brusniak, L., Khorrami, M. R., Fares, E., and Koenig, B., "Comparison of Boeing 777 Landing Gear Noise Simulations with Flight Test Data," paper to be presented at the 27th AIAA/CEAS Aeroacoustics Conference, August 2021.

[17] Khorrami, M.R. and Fares, E. "Toward noise certification during design: airframe noise simulations for full-scale, complete aircraft", CEAS Aeronaut J (2019) 10: 31. doi:10.1007/s13272-019-00378-1.

[18] Koenig, B., Fares, E., Murayama, M., Ito, Y. Yokokawa, Y. Yamamoto, K., and Ishikawa, K., "Lattice-Boltzmann Simulations of the JAXA JSM High-Lift Configuration," AIAA Paper 2016-3721, 2016.

[19] Singh, D., Koenig, B. Fares, E., Murayama, M., Yokokawa, I., and Yamamoto, Y., "Lattice-Boltzmann Simulations of the JAXA JSM High-Lift Configuration in a Wind Tunnel", AIAA Paper 2019-1333, 2019.

[20] Koeing, B., Singh, D., Fares, E., and Wright, M., "Transonic Lattice Boltzmann Simulations of the NASA-CRM in the European Transonic Wind Tunnel", AIAA Paper 2019-3171, 2019.

[21] Vatsa, V., Duda, B., Lin, J, Melton, L., and O'Connell, M., "Numerical Simulation of a Simplified High-Lift CRM Configuration Embedded with Fluidic Actuators" AIAA Paper 2018-3063, 2018.

[22] Fares, E., Duda, B., and Khorrami, M., "Airframe Noise Prediction of a Full Aircraft in Model and Full Scale Using a Lattice Boltzmann Approach", AIAA Paper 2016-2707, 2016.

[23] Khorrami, M., Ravetta, P., Lockard, P., Duda, B., and Ferris, R., "Comparison of Measured and Simulated Acoustic Signatures for a Full-Scale Aircraft with and without Airframe Noise Abatement", AIAA Paper 2018-2975, 2018.

[24] Khorrami, M. R., Fares, E., Duda, B., and Hazir, A., "Computational Evaluation of Airframe Noise Reduction Concepts at Full Scale," AIAA Paper 2016-2711, May-June 2016.

[25] Marié, S., Ricot, D., and Sagaut, P., "Comparison between lattice Boltzmann method and Navier–Stokes high order schemes for computational aeroacoustics," J. of Computational Physics, Vol. 228, pp. 1056-1070, 2009.

[26] Spalart, P. R., Jou, W-H., Strelets, M., and Allmaras, S. R., "Comments on the Feasibility of LES for Wings, and on a Hybrid RANS/LES Approach," Advances in DNS/LES, 1st AFOSR Int. Conf. On DNS/LES, Greyden Press, Columbus, OH, Aug 4-8, 1997.

[27] Spalart, P. "Strategies for turbulence modelling and simulations". International Journal of Heat and Fluid Flow, Vol. 21, pp. 252-263, 2000.

[28] Larsson, J. and Wang, Q., “The prospect of using LES and DES in engineering design, and the research required to get there” Philosophical Transactions of the Royal Society A, Vol. 372, Issue 2022, 2014.
[29] Fares, E., Duda, B., Ribeiro, A.F.P., and Koenig, B., “Scale-resolving simulations using a lattice Boltzmann-based approach” CEAS Aeronautical Journal, Vol. 9, pp. 721-733, 2018, doi: 10.1007/s13272-018-0317-0
[30] Chen, H., Kandasamy, S., Orszag, S., Shock, R., Succi, S., and Yakhot, V., “Extended Boltzmann Kinetic Equation for Turbulent Flows,” Science, Vol. 301, 2003, pp. 633-636.
[31] Chen, H., Teixeira, C., and Molvig, K. “Digital Physics Approach to Computational Fluid Dynamics: Some Basic Theoretical Features”, International Journal of Modern Physics C, Vol. 8, No. 4, pp. 675-684, 1997.
[32] Zhang, R., Shan, X. and Chen, H. “Efficient kinetic method for fluid simulation beyond the Navier-Stokes equation”, Physical Review E, American Physical Society, Vol. 74, Issue 4, October 2006.
[33] Fan, H., Zhang, R., and Chen, H. “Extended volumetric scheme for lattice Boltzmann models” Physical Review E, American Physical Society, Vol. 73, Issue 6, June 2006.
[34] Chen, H., Teixeira, C., and Molvig, K., “Realization of Fluid Boundary Conditions via Discrete Boltzmann Dynamics”, International Journal of Modern Physics C, Vol. 9, No. 8, pp. 1281-1292, 1998.
[35] Chen, H., "Volumetric Formulation of the Lattice-Boltzmann Method for Fluid Dynamics: Basic Concept," Physical Review E, Vol. 58, No. 3, pp. 3955-3963, 1998.
[36] Najafi-Yazdi, A., Brès, G. A., and Mongeau, L., “An Acoustic Analogy Formulation for Moving Sources in Uniformly Moving Media,” Proceeding of The Royal Society of London A, Vol. 467 (2125), 2011, pp. 144–165.
[37] Manoha, E. and Caruelle, B. “Summary of the LAGOON Solutions from the Benchmark problems for Airframe Noise Computations-III Workshop”, AIAA Paper 2015-2846, 2015.
[38] Choudhari and M., Lockard, D., “Assessment of Slat Noise Predictions for 30P30N High-Lift Configuration from BANC-III Workshop”, AIAA Paper 2015-2844, 2015.
[39] BANC-IV workshop: http://aeroacoustics2016.com/banc-iv-workshop/, homepage visited 29,10.2019.
[40] Spalart, P. R., Belyaev, K. V., Shur, M. L., Strelets, M. K., and Travin, A. K., “On the differences in noise predictions based on solid and permeable surface Ffowcs Williams-Hawkings integral solutions,” International Journal of Aeroacoustics, Vol. 18(6-7), pp. 621-646, 2019, doi: 10.1177/1475472x19878934.
[41] Shur, M., Spalart, P., and Strelets, M., “Noise prediction for increasingly complex jets, Part I: Methods and tests”, International Journal of Aeroacoustics, Vol.4, No.3, pp. 213-246, July 2005.
[42] Duda, B., Ferris, R., and Khorrami, M., “Simulation-Based Assessment of a Full-Scale Installed Quiet Landing Gear”, AIAA Paper 2019-2476, 2019.